ELSEVIER

Journal of Chromatography A, 905 (2001) 163–173

JOURNAL OF CHROMATOGRAPHY A

www.elsevier.com/locate/chroma

TiO_2 colloidal suspension polydispersity analysed with sedimentation field flow fractionation and electron microscopy

Philippe J.P. Cardot[a,*], Sousan Rasouli[a], Philippe Blanchart[b]

[a]*Laboratoire de Chimie Analytique and Bromatologie, Faculté de Pharmacie, Université de Limoges, 2 Rue du Dr Marcland, F-87025 Limoges, Cedex, France*

[b]*Groupement d'Etude des Matériaux Hétérogènes, Ecole Nationale Supérieure de céramique industrielle, 47 Avenue Albert Thomas, F-87065 Limoges, Cedex, France*

Received 8 June 2000; received in revised form 15 September 2000; accepted 18 September 2000

Abstract

Sedimentation field flow fractionation (SdFFF) operated at multi gravitational field is used to analyse a highly polydisperse TiO_2 colloidal suspension. From the initial sample, time dependent eluted fractions are collected and submitted to electron microscopy (EM) shape and size analysis. To assess the accuracy of FFF in determining the average size of the different fractions, these are re-introduced into the channel by means of two different procedures, the on-channel concentration of the fractions and the direct re-injection of pre-concentrated fractions (DRI). Both methods appear accurate to determine the average size of every fraction, associated to a lower recovery in the case of DRI. The fractogram band spreading characteristics of the re-introduced fractions are correlated to the particle size distribution measured by EM. After density determination of fractionated particles, the fractogram is calibrated in terms of size and size distribution using data obtained from EM for each fraction. Quantitative analyses, based on particle counting showed high recovery (80–90%) of the eluted species. However, this loss limited the possibility to extend signal information to a quantitative one.

Keywords: Colloids; Polydispersity; Field flow fractionation; Electron microscopy; Titanium oxide

1. Introduction

Sedimentation field flow fractionation (SdFFF) operated at multi gravitational field is an analytical methodology applicable to the separation of a large variety of colloids [1–5]. The separation principle and mechanism is described as ''Brownian'', in which selective elution is provoked by the combined action of a flow, the colloid Brownian motion and an external field applied perpendicularly to the accumulation wall of the ribbon-like channel [6,7].

In this report we have investigated the separation power of SdFFF on a very polydisperse TiO_2 colloidal sample. Eluted fractions were collected and submitted to two different types of characterisation techniques. The first one is electron microscopy (EM) [8]; fractions mean size and dispersity, i.e., the standard deviation of the population size distribution (σ-size), can be therefore obtained, leading to a polydispersity index [9]. In a second step we have

*Corresponding author. Tel.: +33-5-5543-5857; fax: +33-5-5543-5859.

E-mail address: cardot@unilim.fr (P.J.P. Cardot).

0021-9673/01/$ – see front matter
PII: S0021-9673(00)00973-0

investigated two FFF re-injection procedures of the first run collected fractions. One has already been experienced by Giddings [10] and requires sophisticated injection design and methodology it is designed as on-channel concentration (OCC). The second, consists of direct re-injection (DRI) of the fractions pre-concentrated by centrifugation.

Sample polydispersity analyses of colloids have gained an increased interest, particularly when multi angle light scattering detectors are used. Examples obtained from Flow FFF were recently published [11]. Theoretical treatment of polydispersity analyses in FFF was recently published by Schure [12]. In the following, a pure experimental approach was chosen using size analysis as well as population dispersity measurements by means of EM correlated with fraction re-elution measured characteristics of fractograms obtained from re-injection FFF procedures.

From EM, it is possible to calculate, by means of image analysis not only the average size of the population (of the collected fraction) but also its polydispersity. Equivalent access to polydispersity measurements in FFF may be obtained from the re-injection procedures, to provide average size and dispersity information using retention and band spreading characteristics [13]. Dispersity information obtained from band spreading data of re-eluted fractions can be therefore calibrated by means of those obtained from EM.

2. Experimental

2.1. TiO_2 sample

A TiO_2 Powder TR-HP2 (Structure Rutil) from Bayer (Bayer, Fosses St. Witz, France) was used. The manufacturer specifications claimed an average diameter of 0.5 μm determined by velocimetric techniques. All suspensions were performed using the separation carrier phase as solvent.

2.2. SdFFF system

The SdFFF device used in this report is laboratory designed and has already been technically described [14]. It must be noticed, that this SdFFF channel presents a major difference with all those described in the literature or commercialised. This difference is linked to the injection tubing, which is connected to the channel via the accumulation wall. The channel dimensions are $78.5\times0.8\times0.025$ cm. The system void volume, which includes the connection tubing, injection and detector volumes, was measured at 1.80 ± 0.05 ml ($n=15$, 2σ) using a 10% (w/w) Dextran solution (Dextran D-4026, Sigma–Aldrich, Poole, UK). The channel was positioned 14 cm from the rotation axis. A Gilson Model 302 (Gilson, Mideltown, WI, USA) HPLC pump was used to produce the carrier phase flow. The carrier phase is a mixture made of 0.05% (v/v) FL-70 (Fisher Scientific, Elancourt, France) and 0.001 *M* KNO_3 (P-6083, Sigma–Aldrich) in doubly distilled water.

Sample introduction were performed via a 7525 Rheodyne (Cotati, CA, USA) valve whose injection loop can be set at 15 μl for DRI and 75 μl for the first fractionation. Sample detection was performed with an ICS differential refractometer detector Model ICS M8110 (Société ICS, Lauganet, France). Refractometric signal was recorded and digitised by means of a computer system already described [14]. Crude sample FFF injection conditions were 75 μl of a 3% (w/w) TiO_2 colloidal suspension with a 17 min/14.1 *g* stop flow injection procedure. Elutions were performed at a 1 ml min^{-1} flow and at 4.06 *g* centrifugal field.

2.3. FFF re-introduction procedures

OCC procedure [10]: for each fraction the whole 3 ml collected volume was fed into the channel at 0.15 ml min^{-1} flow-rate under an established field of 56.4 *g*. This feeding step was made possible, replacing the injection valve of classic FFF system by a Microperpex peristaltic pump from LKB (Bromma, Sweden) to introduce the sample into the channel. For the elution step, field strength was reduced to 4.06 *g* and flow-rate increased to 1.5 ml min^{-1}

DRI procedure: the whole fraction was concentrated in 10 μl by a 10 min/3000 *g* centrifugation. Sonication (2 min) and vibration (2 min) were applied to the resulting 10 μl to limit aggregation [15]. The whole fraction was then directly analysed. Stop flow injection and elution conditions of 17 min/14.1 *g* and 1.5 ml min^{-1}/4.06 *g* were applied.

2.4. Granulometric analyses

Crude sample and collected fractions photos were analysed by means of an Hitachi (Tokyo, Japan) S-2500 scanning electron microscope to obtain size average and polydispersity characteristics. A Sedigraph 5100 (Micromeritics, Norcross, GA, USA) was used to determine the mass distribution. Crude sample average density was measured by means of an helium pycnometric method using a multivolume pycnometer 1305 (Micromeritics). Direct microscopic particle counting was performed with an optical microscope Leica DM LB (Leica microsystèmes, Reuil-Malmaison, France) and 1 μl Malassez haemocytometer counting device (Preciss, Paris, France).

EM size algorithms: four different size algorithms were used. The first one (sphere-like) calculate particles diameter at different angles (60°) — six different diameters calculated — and returns the average diameter. This algorithm assimilates the particles to sphere. If ovoid particles are to be considered, three other algorithms were used. One determines the smallest (particle breadth) diameter of the particle, the second determines the greater and smaller diameters and returns an average value (mean size). The third one determines only the greater diameter of the particle. Fraction size distributions are described in terms of fraction size standard deviation and systematically designed as ''size dispersity''.

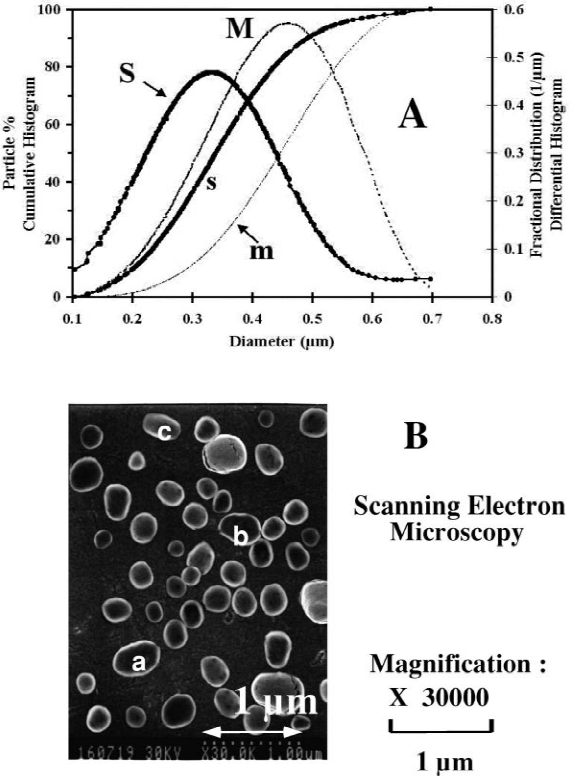

Fig. 1. TiO_2 particle size characteristics. (A) Cumulative (s and m) and fractional (m and M) size distributions of TiO_2 particles. Curves (s and S) are related to the number distribution and curves (m and M) to the mass distribution. (B) Electron microscopy profile of TiO_2 sample (magnification ×30 000), the photo shows almost 50 particles. Curve s, was determined using eight different slides of the sample, whose particle size, and disperisity was calculated using image analysis. The particle shape varies from quasi-spherical to ellipsoid (a, b, c), these being also the bigger.

3. Results and discussion

3.1. Granulometric characterisation of the TiO_2 sample

In order to fit with the information provided by the TiO_2 manufacturer, a cumulative distribution, expressed in particle mass was obtained [16] using a velocimetric method (Sedigraph) as shown in Fig. 1A, curve m. The resulting mass differential histogram, curve M, led to an average particle diameter of 0.49 μm. A continuous distribution is observed over a 0.1–0.7 μm range indicating the high polydispersity [9] of the sample (polydispersity index=30%, standard deviation to average value ratio expressed in percentage). All these values match closely the ones claimed by the manufacturer. It is also possible to describe the sample by means of a number distribution against size. Particle size distribution was performed by EM measurements and subsequent image analysis from series of 350 particles. A picture of the raw sample is shown in Fig. 1B. If a large majority of particles appeared spherical, a small percentage (lower than 7% in number) showed ellipsoidal shape, these particles being also the bigger ones as evidenced by particles a, b and c of Fig. 1B. Cumulative and differential histograms [16] obtained from image analysis are shown in Fig. 1A curves s and S. The resulting particle size analysis

led to an average particle size of 0.32 μm and a continuous size distribution between 0.1 and 0.6 μm. The different granulometric determination techniques indicates a 30–40% polydispersity index. In the followings, all size and dispersity characteristics are given from EM. Sample density was obtained via a helium pycnometric method and measured at 4.27 ± 0.02 g ml^{-1} ($n=6$, 2σ) g ml^{-1}.

3.2. TiO_2 SdFFF elution

Stop flow injections of the crude TiO_2 sample led to the characteristic monomodal profiles shown in Fig. 2A. Systematic injections of the same sample led to very reproducible profiles. Such reproducibility has already been observed during systematic validation process of this SdFFF system [14] for micron-sized species. The 3% (w/w) suspension concentration was chosen to provide significant particles in the different collected fractions for image analyses, and a signal-to-noise ratio as large as possible compatible with accurate peak profile characteristics measurements. In a first step particle number recovery was performed via direct microscopic analysis. For that purpose, 75 μl of the sample was eluted and the whole eluted sample, over 100 ml, collected (sample A). By centrifugation, sample A volume was reduced to 1 ml. An identical crude sample volume was diluted up to 1 ml (sample B).

A series of direct microscopy analyses via the Malassez device (haemocytometer) allowed to compare the particle concentrations in samples A and B. Recovery expressed in particle number was calculated as the number of counted particles ratio of samples A versus B, $85\pm7\%$ ($n=5\times2$, 2σ) recovery were obtained.

From the elution profiles shown in Fig. 2A, five fractions of identical volume (3 ml) were chosen at different elution times and collected as shown in Fig. 2B. Average particle size can be determined using FFF related equations [17] assuming a known and constant density over the whole TiO_2 population. Image analyses of the fraction slides shown in Fig. 3 were also performed. The results from both sizing methods are shown in Table 1, with retention and collected volumes characteristics. As a consequence, at any retention time along the fractogram, an

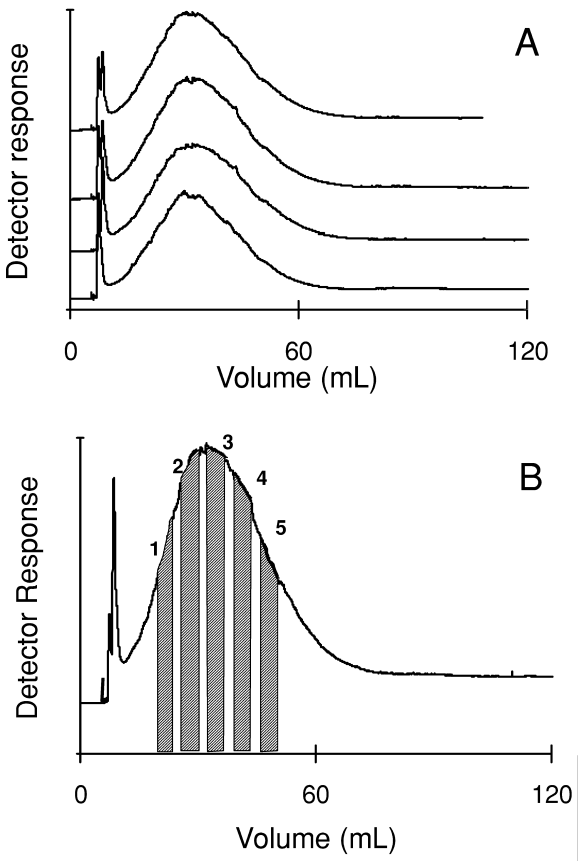

Fig. 2. TiO_2-SdFFF fractograms. (A) SdFFF fractograms of TiO_2 sample using refractometric detection. Detector attenuation 1/100–10 mV full scale signal, reference: carrier phase. Injection and elution conditions described in text. Legend 1, 2, 3, 4 corresponds to the successive elution of an identical sample (1 to 4). (B) Elution volume of the 5 (3 ml) collected fractions. Injection and elution conditions described in text, (a, b, c ellipsoid particles).

average size can be deduced. It must be noticed, that 0.6 μm diameter (FFF sizing) particles are related to an elution volume (>100 ml) corresponding to the absence of signal as shown in Fig. 2A and B. The accuracy of the FFF selective separation of subpopulations of different sizes is confirmed when the diameter based selectivity curve is analysed by EM as shown in Fig. 4. The diameter based selectivity curve is defined as the logarithm of the retention time against the logarithm of the size determined by EM. The regression curve of the first four fractions is associated to a slope (the size based selectivity, Sd)

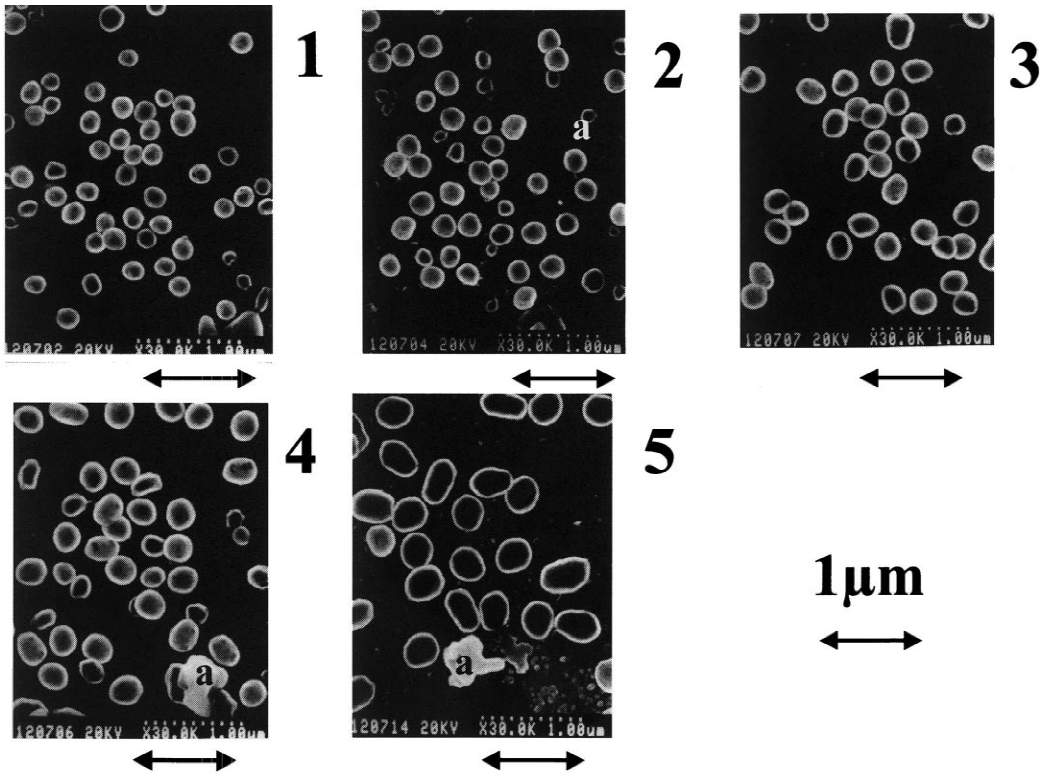

Fig. 3. Electron microscopy photos of the collected fractions. Electron microscopy experimental conditions described in Fig. 1 legend. Associated photo black lines, are used to calibrate each slide and correspond to 1 μm. Collected fraction characteristics given in text. ([a] particles are EM artefacts).

whose absolute value $|Sd|=2$, a value which differs (30%) from the theoretical one [1,18]. This difference is caused by the high sample quantity needed for accurate microscopy size analysis, therefore this fractogram was obtained in sample overloading conditions.

The last fraction average size appeared biased because of its ellipsoidal shape as shown in Figs.

Table 1
Collected fractions retention characteristics[a]

Fraction	Retention volume (ml)	3 ml fraction volume	Retention ratio	FFF* calculated diameter ±0.005 μm	EM** measured diameter (n=350) ±0.01 μm
1	16.5	15–18	0.108	0.236	0.22
2	23.5	22–25	0.076	0.265	0.24
3	28.5	27–30	0.063	0.283	0.28
4	34.5	33–36	0.052	0.300	0.31
5	41.5.5	40–43	0.043	0.320	0.36* (0.33–0.40)

[a] Retention ratio calculated from void to retention volumes ratio. *''FFF'' equivalent diameter defined as the average particle hydrodynamic diameter calculated from Ref. [8], assuming a 4.27 density, and a $|Sd|=3.0$ theoretical size selectivity. **EM measured diameter calculation were performed using a ''Spherical-like'' sizing algorithm.

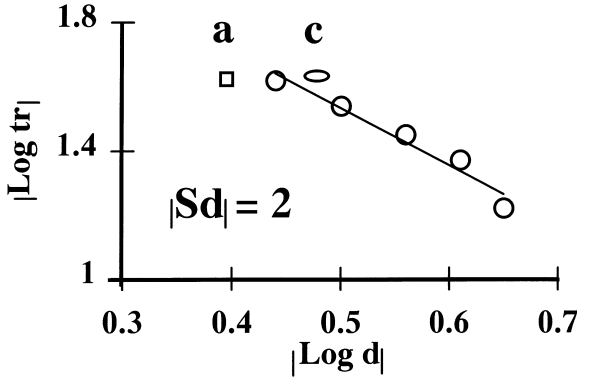

Fig. 4. Size related selectivity of TiO_2 in SdFFF. Fraction average size expressed in μm. Abscissa expressed as the absolute value of the logarithm of the size. Elution time expressed in minutes, (a, b, c) correspond to average size of fraction calculated using different size determination algorithms as described in text.

3–5. However from this first experimental stage, it is possible to calibrate the SdFFF system for TiO_2 size determination from SdFFF retention dependent analysis. One must notice from Table 1 data, that sizes measured from EM are not linearly correlated to those calculated from FFF equations, justifying the Fig. 4 calibration curve. In particular, diameters obtained from FFF and displayed in Table 1, were calculated assuming the hypothesis of [Sd]=3

However, systematic image analysis for granulometric characterisation on every eluted fractions is time consuming. Another methodological approach consists in determining the average size from fraction reintroduction into the channel and subsequent peak profile analysis. This is made possible because of the very high selectivity of the SdFFF separation in the case of TiO_2 colloid as shown from Table 1 and Fig. 4 data. Radius differences of 10–20 nm were evidenced from the five fractions analyses. which corresponds to a relative size difference of 10–15%. It is therefore possible to control and extend the potentialities of fraction reintroduction procedures using the general methodology previously described.

3.3. SdFFF reintroduction procedures for retention dependent size determination

All the collected fractions are reintroduced into the channel by means of two different protocol. The first

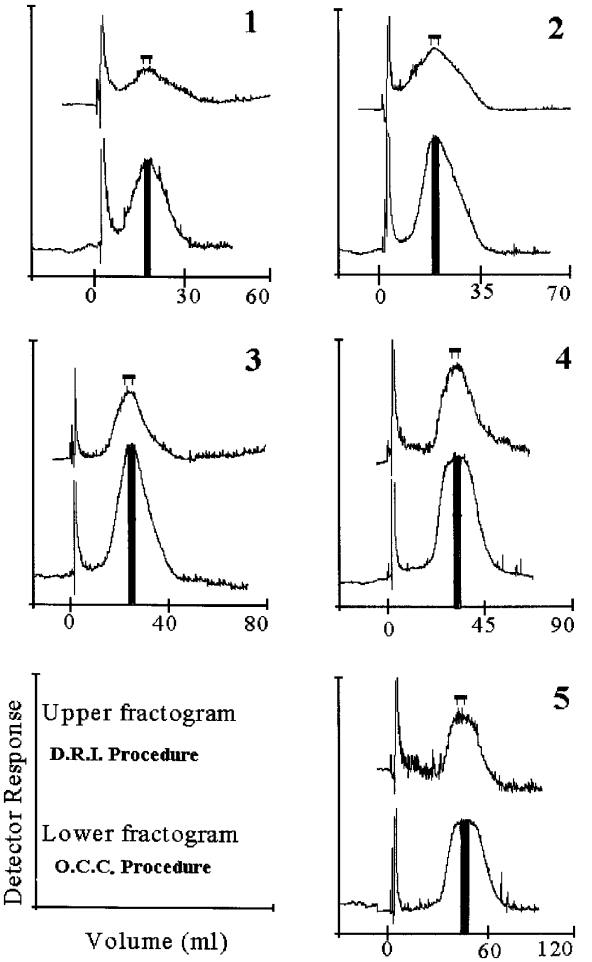

Fig. 5. Reintroduction procedures fractograms. Experimental conditions described in text. Refractometric sensitivity. Detector attenuation 1/200–10 mV full scale signal. Fractograms series 1–5 corresponds to the five fractions of Fig. 2B. Upper fractogram dots placed at peak summit as well as lower fractograms bars showed the collected faction submitted to EM analyses (Table 3, Fig. 6).

one is the OCC procedure already described by Giddings et al. [10] and the second (DRI) is a simple volume reduction of the solvent from 3 ml to 10 μl. For the OCC procedure [10] external field and flow-rate characteristics of the ''Feeding Step'' [10] (large sample volume introduction method) have been chosen to obtain a measured apparent retention ratio very close to the actual one. It must be noticed at that stage that, because of the reproducibility of the FFF elution, we can assume that every fraction will

reproducibly encompass the same amount of particles either in terms of mass or in terms of particle number. For the DRI procedure, collected sample were concentrated by centrifugation with most solvent removed and the remaining 10 μl suspension re-injected in the separator. Identical peak profile analysis was thus performed. Therefore comparison can be made for fractions collected at the same retention time but reintroduced by the different protocols. Fractograms obtained for each fraction with both re-injection procedures are shown in Fig. 5. From experiments described in Fig. 5 series of 0.5 ml fractions centred at the retention time were collected and submitted to EM analysis. Slides obtained from the OCC procedure are shown in Fig. 6. Table 2 displays data for each fraction and both re-injection procedures, the retention ratio, the FFF calculated size and the EM measured average size. Very good correlation is obtained when calculated size obtained from retention data of both re-injection procedures are compared, leading to the conclusion that they are equivalent in term of size determination. Good correlation also is observed when these EM data are compared to those of Table 1.

For each re-eluted fraction it is possible to determine the second run recovery using the methodology already described above. An average fraction recovery expressed in particle number of 89±8% (n=15[5×3], σ) was obtained for the OCC procedure, a fraction recovery of 69±9% (n=15[5×3], σ) was obtained for the DRI method. It is observed that recovery differences (20% in number) led to fractogram area differences as shown in Fig. 5 fractogram series. Fortunately these recovery differences do not significantly modify the average size determination by EM. The loss is not caused by any pre-concentration treatment but appeared to be connected to the different primary relaxation step used in OCC and DRI.

Table 2 data allows to calculate the size selectivity [Sd] correlating the FFF retention characteristic of every fraction to their EM measured average size. [Sd] values very close to 3 are found showing an equivalent capacity of both reintroduction procedures to determine the sample fraction average size as theoretically predicted [16]. One must notice that accurate size selectivity slope [|Sd|=3]is obtained after re-elution of the fractions.

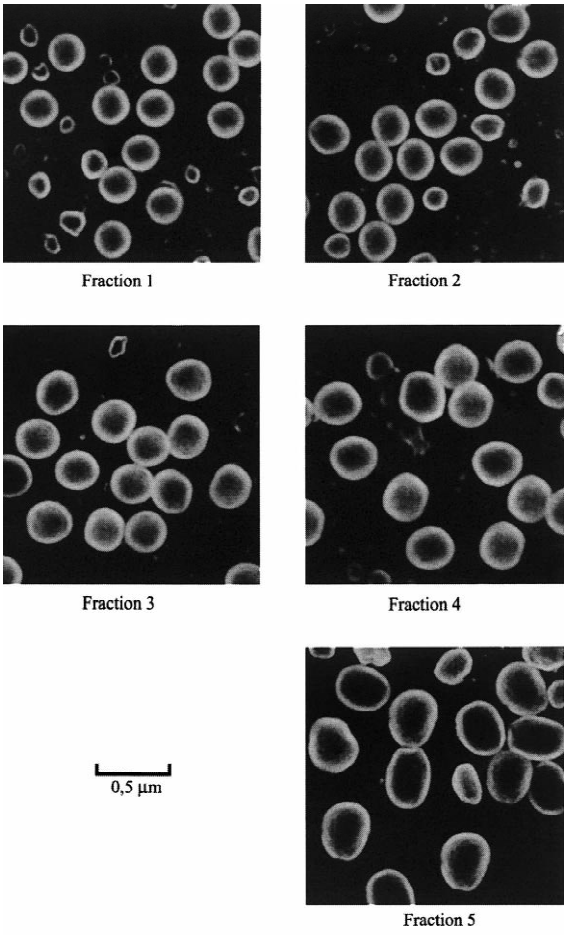

Fig. 6. Examples of EM photos series collected after on-channel concentration re-elution. Collected samples images 1–5 correspond to 0.5 ml fractions centered at retention volume.

In terms of size determination, both reintroduction methodologies appeared accurate, however the low signal-to-noise ratio observed for the DRI procedure lead to the conclusion that the OCC one should be preferred, in particular if very diluted crude materials are to be analysed. The re-elution of diluted sample will drive to an over dilution of the sample. The reduced amount of sample particles in re eluted fractions available for image analysis leads to possible accuracy bias as shown by the EM measurement distribution observed when Tables 1 and 2 data are compared. It is observed that Table 2 EM size are systematically majored compared to those of Table 1.

Table 2
Re-eluted fraction characteristics[a]

Fraction	Retention ratio		FFF* calculated average diameter ±0.009 μm		EM** measured average diameter* ±0.013 μm	
	DRI	OCC	DRI	OCO	DRI	OCO
1	0.093	0.101	0.250	0.243	0.230	0.224
2	0.067	0.072	0.278	0.272	0.252	0.252
3	0.062	0.066	0.286	0.280	0.280	0.284
4	0.049	0.047	0.310	0.315	0.327	0.325
5	0.036	0.035	0.342	0.348	0.380*	0.370*

[a] Calculation methods described in Table 1 legend. * and ** as in Table 1 legend.

The fractograms of Figs. 2 and 5 as well as the EM images of Figs. 3 and 6 have been, so far, interpreted only in terms of retention and average size characteristics. Elution profile band spreading parameters can be used to assess each fraction polydispersity values. Dispersity data collected from Fig. 6 (OCC image analysis) as well as DRI fractions (EM images not shown) will be used to correlate the particle size and dispersity obtained by the SdFFF system(see Table 2).

3.4. SdFFF and polydispersity analyses

3.4.1. Fraction polydispersity

Size dispersities of the five fractions after the crude sample first run are obtained from image analysis whose slide examples are given in Fig. 3. Mean and dispersity values obtained for each fraction are calculated; data are shown in Fig. 7. The image analysis algorithm consider particles as spheres [18], and size distributions are shown in Fig. 7 (curves 1–5 correspond to the different fractions). Using the ''sphere-like'' image analysis algorithm for faction 5 will generate biased results with an average value of 360 nm. The ellipsoidal particles clearly evidenced in Fig. 3 slide 5, are therefore measured using their breadth as principal dimension. In that case, the fraction 5 particle size distribution is plotted as curve 5a, and the resulting measured size is 327 nm. A third size analysis of fraction 5 is determined using an algorithm which calculates the mean size of each particle as plotted in Fig. 7 as curve 5b (370 nm). To complete the particle size distribution of fraction 5, curve 5c describes the pattern observed assuming an image analysis using the greater dimension of the particles (420 nm). Mean and dispersity characteristics appeared very different depending on the measurement algorithm showing clearly the difficulty of shape and size analysis. However, with the hypothesis of a ''sphere-like'' sizing methodology it is now possible to correlate dispersity data of Fig. 7, curves 1–5, to the ones provided by a classical fractogram profile analysis.

3.4.2. Retention ratio and possible dispersity calibration

In a first step, retention characteristics can be correlated with EM measured dispersity patterns, successful correlations are obtained when retention characteristics before and after re-injection are analysed versus fractions dispersities σ-size (1) described in Table 3. σ-size (1, 2, 3) is the size

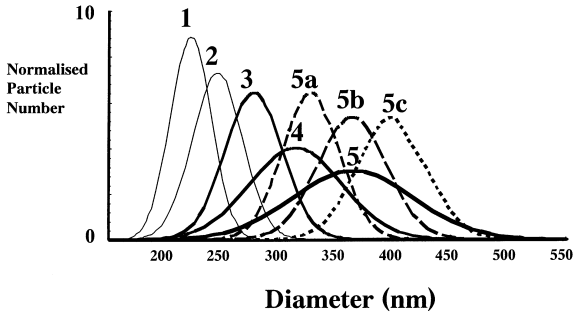

Fig. 7. TiO_2 collected fractions size characteristics. Collected fraction size and dispersity characteristics. Differential histograms are normalised (identical area), and correspond roughly to 150 particles. Image analysis algorithm assuming spherical particles was used for curves 1–5. curves 5a, 5b, 5c were determined using modified algorithms whose principles are described in text.

Table 3
Crude and fractions samples size dispersities and density characteristics[a]

Fraction	Size standard deviation measured from Fig. 3 data (nm) σ-size (1) (n=350)	Size standard deviation measured after DRI elution (nm) σ-size (2) (n=150)	Size standard deviation measured from Fig. 6 data (nm) σ-size (3) (n=150)	Density measurements ±0.03
1	18	12	12	4.27
2	22	17	15	4.26
3	26	25	25	4.27
4	40	36	35	4.27
5	53* (a=25, b=30, c=30)	43	41	4.25

[a] Size standard deviations calculated from Image analyses data (n=150). Density determination method described in text.

standard deviation measured from EM, and depends on the fraction sample used (1, 2, 3)

Density determination of the five fractions shown in Figs. 2B and 3 are described in Table 3, they all showed analogous values confirming the hypothesis of an homogenous density of the crude sample. However, the relative low amount of available material limited the accuracy of the measurements.

It must be noticed, as shown in Table 3, that the collected fraction at peak summit after reintroduction, led to EM measured dispersities lower than σ-size (1). This, shows second step purification potentialities as these fractions appeared less disperse (Table 3, 2nd and 3rd columns) than the preceding ones (Table 3, 1st column).

3.4.3. Elution profile band spreading probes and particle polydispersity.

Band spreading characteristics [like height equivalent to a theoretical plate (HETP) and second moment of the eluted peak], must be at evaluation of the fractograms shown in Fig. 5. In order to extract specific band spreading information from fractogram data (separator, non equilibrium and sample polydispersity contributions) a specific methodology must be taken into account, the which has been established by Giddings et al. [17] and was recently applied successfully for gold nanometric suspensions [19].

To determine the non ideal contributions (ΣHj) to plate height that are not due to the polydispersity of the sample, injections of salicylic acid (1 g/l) were run at five different flow-rates (0.4, 0.6, 0.8, 1, 1.25, 1.5 ml/min) and the resulting plate heights calculated. The resulting linear regression lead to a slope of 5.07 mm min/ml and a zero flow-rate HETP intercept of 2.23 mm (R=0.99). An analogous methodology was applied to the calculation of (ΣHj) for the five re-injected fractions at three different flow-rates (0.5, 1, 1.5 ml/min). Particle size standard deviation are therefore calculated [17,19] and results are shown in Table 4. When Tables 3 and 4 data are compared very good agreement is found between fraction dispersity obtained by SdFFF and EM. However, from Tables 3 and 4, it is observed that HETP dependent size dispersity appeared less accurate when the fractions of bigger size (fractions 4 and 5) were considered. These EM measured size polydispersity discrepancies with FFF related data can be attributed to the difficulty of an accurate EM size measurement when non spherical particles are involved.

Table 4
Band spreading characteristics and sample dispersity[a]

Fraction	HETP (mm) at zero flow-rate		Particle standard deviation calculated from HETP	
	DRI	OCO	DRI (nm)	OCO (nm)
1	18.5	19.3	12.2	12.26–12.9
2	28.6	23.4	16.8	14.6–16.2
3	55	58	23.1	24
4	85	NC*	37.5	NC*
5	NC*	NC*	NC*	NC*

[a] HETP calculated from first and second moments of Fig. 5 fractograms. Fig. 5 samples were run at three different flow-rates. From HETP measurements at different flow-rates, C and ΣHj were obtained from linear regressions. NC* in fractions 4 and 5 signs low linear regression correlation coefficient (<0.9).

4. Conclusion

The experimental results obtained in this report show clearly that size and dispersity measured values obtained from FFF data have to be taken with precaution. Real proofs of the separation are given by independent methods like EM. It appeared that size based selectivity [Sd] was two from the first elution and three after re-elution (whatever the re-injection method). The injection of relatively large quantities of sample led to overloaded fractogram which biased the effective SdFFF selectivity of the first run [20,21].

The size selectivity of three experimentally found with re-injection procedure indicated that the elution mode of every fraction is strictly Brownian. This procedure, strictly based on elution fraction collection is at difference with the one described by Park and Lee [22] for rod-shape chromium oxide, eluted on the ''Lift'' mode, which was partially based on FFF related sizing procedures. The methodological procedure described in this report is also at difference with the one using field programmed elution described in the early 1980s by Kirkland et al. [23], whose size distribution were also described on the unique basis of FFF related equations.

Size determination by re-injection procedures can be so far considered as classic, it is demonstrated that the OCC one provided a signal which was easier to interpret. It is also demonstrated that both re-injection procedures led to accurate size determination. The size dispersity determination of every fraction made by EM, led to polydispersity patterns, which can be correlated to fractogram characteristics. It has been necessary to calibrate the SdFFF/TiO_2 system in term of mass transfer band broadening contribution to extract the effective sample dispersity contribution to HETP (ΣHj).

Both re-injection procedures related FFF peak characteristics measurements appeared accurate to determine the TIO_2 size and polydispersity patterns for the three first fractions. Accurate average values of factions 4 and 5 have been also determined using FFF technique. However particle size dispersity of fractions 4 and 5 calculated from FFF and EM appeared biased, justifying the systematic use of independent sizing method coupled to FFF. In term of separation process the methodological choice will depend on the sample. If very diluted samples are analysed, the OCC procedure appears to be the most effective one. If large amounts of crude samples are available, DRI procedure will provide valuable information. The trapping of sample in the separator, which limits recovery is critical if FFF is to be used for assay purpose. If it is possible to evaluate the reversible trapping by systematic post elution flushing at field stopped with carrier phase of different characteristics, the assessment of irreversible trapping is more complex.

Acknowledgements

Dr. Josef CHMELIK is acknowledged for helpful discussions and English corrections.

References

[1] J.C. Giddings, Science 260 (1993) 1456.
[2] K.D. Caldwell, G. Karaiskakis, J.C. Giddings, J. Chromatogr. 215 (1981) 323.
[3] J.G. Weers, R.A. Arlaukas, Langmuir 11 (1995) 474.
[4] A. Athanosopoulous, G. Karaiskakis, Chromatographia 40 (1995) 734.
[5] C. Contado, G. Blo, F. Fagioli, F. Dondi, R. Becket, Colloids Surf. A: Physicochem. Eng. Asp. 120 (1997) 47.
[6] J.C. Giddings, G. Karaiskakis, K.D. Caldwell, M.N. Myers, J. Colloid. Interface Sci. 92 (1993) 66.
[7] F.S. Yang, K.D. Caldwell, J.C. Giddings, J. Colloid. Interface Sci. 93 (1993) 115.
[8] M. Coster, J.L. Chermant, Precis d'Analyse d'Images, Ed. Du CNRS, Paris, 1989.
[9] J.M. Métreau, S. Gallet, Ph.J.P. Cardot, V. Le Maire, F. Dumas, A. Hernvann, S. Loric, Anal. Biochem. 251 (1997) 178.
[10] J.C. Giddings, G. Karaiskakis, K.D. Caldwell, Sep. Sci.Technol. 16 (1991) 725.
[11] P.J. Wyatt, D.N. Villalpando, Langmuir 13 (1997) 3913.
[12] M.R. Schure, J. Chromatogr. A 831 (1999) 89.
[13] J.C. Giddings, F.S. Yang, J.Colloid. Interface Sci. 105 (1985) 55.
[14] E. Assidjo, T. Chianea, M.F. Dreyfuss, Ph.J.P. Cardot, J. Chromatogr. B 709 (1998) 197.
[15] J.C. Giddings, M.N. Barman, H. Li, J. Colloid. Interface Sci. 132 (1989) 554.
[16] J.S. Reed, Introduction to the Principles of Ceramic Processing, Wiley–Interscience, New York, 1988.
[17] J.C. Giddings, Y.H. Yoon, K.D. Caldwell, M.N. Myers, M.E. Hovingh, Sep. Sci. 10 (1975) 447.

[18] P. Robert, J. Melcion, F. Le Deschault De Monredon, Powder Technol. 90–92 (1997) 141.
[19] S. Anger, K. Caldwell, H. Niehus, R.H. Mûller, Pharm. Res. 16–11 (1999) 1743.
[20] G. Karaiskakis, M.N. Myers, K.D. Caldwell, J.C. Giddings, Anal. Chem. 53 (1981) 1314.
[21] S. Rasouli, Thèse d'Université, Université de Limoges, 2000
[22] Y.H. Park, D.W. Lee, M.M. Moon, Instumentation Sci. Technol. 25–2 (1997) 133.
[23] J.J. Kirkland, W.W. Yau, W.A. Doerner, J.W. Grant, Anal. Chem. 52 (1980) 1944.